List of Symbols Used in This Paper

Symbol	Definition
a_i	activity of species i
x_i	concentration of species i
p_i	partial pressure of species i
γ_i	Raoultian activity coefficient of species i
f_i	Henrian activity coefficient of species i
μ_i^α	chemical potential of species i in α phase
μ_i^β	chemical potential of species i in β phase
E_A	deposition potential of A
E_B	deposition potential of B
E_S	potential at which A and B are codeposited
ΔE_B	$E_B - E_A$
ΔE_S	$E_S - E_A$
ΔG_A^r	Gibbs energy to reduce A from AX
$\Delta G_{A,B}^{mix}$	Gibbs energy of mixing A and B
G_i°	Gibbs energy of species i in its standard state
G_i^l	Gibbs energy of species i in the liquid state
ΔG_i^{ss}	$G_i^\circ - G_i^l$
ρ_i	Wagner-Allanore activity coefficient of species i
χ_i	concentration of species i relative to another species

Non-Standard State Thermodynamics of Metal Electrodeposition

WAGNER Mary-Elizabeth, ALLANORE Antoine

Department of Materials Science and Engineering, Massachusetts Institute of Technology, Cambridge, United States of America

Abstract

Development of new high temperature electrolytes is hindered by lack of information about their thermodynamic solution properties, which must be determined through experiments or modeling. Current models, however, are unable to accurately predict the behavior of the complex multicomponent liquids that make up such electrolytes, and gathering sufficient experimental data for a full analysis is lengthy and expensive. Even if the properties of an electrolyte are well-determined, the link between their thermodynamics and the extent of codeposition that will occur during electrolysis remains unclear. Previous endeavors aimed at linking the difference in deposition potential ΔE of two elements to their codeposition behavior focused on binary cathode alloys that formed ideal solutions. Herein, this approach is generalized to multicomponent cathodes exhibiting real solution ($a_i \neq x_i$) behavior. Through this methodology, targeted experimental data and classical Gibbs energy curves can be used in combination to map out the thermodynamic nature of complex electrolytes. To facilitate this effort, a new thermodynamic reference state for activity is derived that allows one to determine electrolyte activities directly from ΔE. The merits of this approach are tested against experimental case studies and compared to traditional standard state assumptions.

Keywords: thermodynamic modeling; high-temperature electrolyte; separation; codeposition

1. Introduction

Production of metal by electrochemical means is an attractive pathway towards a greener metals industry because electrical energy is used directly for reduction. It is currently the method of choice for production of reactive metals, such as aluminum, magnesium, and the rare earths, and it is widely used for winning and refining other metals such as zinc, nickel, copper, silver, and gold. Except in notable cases, such as praseodymium-neodymium production from a mixed oxide [1], the electrolyzed product tends to be a nearly pure metal. Purification tends to be achieved through either pre-processing to ensure a pure electrolysis feedstock, as in the Bayer process for aluminum production [2], or by carefully selecting a supporting electrolyte insoluble to unwanted species, such as silver and gold in copper anode electrorefining [3].

Recently, new electrochemical technologies are pushing the boundaries of processing conventions. Novel high temperature electrolytes such as molten sulfides [4, 5] and oxides [6] generally have greater solubility for a wider range of elements than their aqueous counterparts. Furthermore, being novel, these electrolytes have many unknown properties which cause difficulty when trying to optimize for selectivity. In these cases, the purity of the final metal product cannot be guaranteed a priori, and many experiments are required to effectively develop the new technology. Challenges with maximizing cathode purity are not limited to emerging technologies, and are of great interest in recycling technologies, particularly in the area of nuclear waste where it is not practical to have multiple separate pre-processing steps [7].

In cases where multiple reduction reactions may occur, little is known about the quantitative link between electrolyte chemistry and cathode product [8], and the electrochemist is either forced to return once more to extensive experimentation or make simplifying assumptions. One such common assumption maintains that if two species are further than 200mV apart on the standard state electrochemical series, then the more reactive species will not contribute at all to the reduction reaction. Conversely, if the standard state reduction potential of two

species are closer than 200mV, codeposition will occur [9, 10]. The major issue with this assumption is its use of pure standard state (a=1) thermodynamic convention, which neglects all effects of concentration and chemical interaction and treats both the electrolyte and the cathode as if they were completely pure. If the concentrations of the species in the electrolyte and cathode are known, the electrochemical series may be adjusted to an *ideal* series. For an oxidized species AX being reduced to metal A and gaseous X such that:

$$A^{n+} + ne^- \rightarrow A \tag{1}$$

$$X^{n-} \rightarrow X + ne^- \tag{2}$$

we can find its ideal decomposition potential via the equation:

$$E^{id} = E^\circ - \frac{RT}{nF} \ln \frac{x_A p_X}{x_{AX}} \tag{3}$$

Where E° is the standard state decomposition potential of AX for a system containing x concentration of A and AX, and a partial pressure p of anodic product X. Although this formalism improves upon standard state, it does not take into account interactions between AX and other species in the electrolyte, or A and other metals in the cathode. Although certain metallic systems can be approximated as nearly ideal, most electrolytes are eutectic systems with interactions that have significant deviations from ideality. These interactions, typically represented by the Raoultian activity coefficient (γ), are particularly important when one considers the fact that in commercial electrolytic processes, the supporting electrolyte is present in far greater concentrations than the electroactive species. For example, in the Hall-Heroult process, Al_2O_3 is present in the range of 2-3 $wt\%$, dissolved in a cryolite supporting electrolyte [11]. Such concentrations are common across other technologies, such as rare earth electrowinning [12]. At these concentrations, the molecules of electroactive species are completely surrounded by molecules of supporting electrolyte (i.e. solvated): an alumina-cryolite interaction is statistically far more common than an alumina-alumina interaction. Therefore, the effect the supporting electrolyte has on the

chemistry of the electroactive species must be considered, and the assumption of standard state behavior can no longer be used. In aqueous electrochemistry, the effect of the electrolyte on electrochemical behavior can be captured in the activity of the proton, as documented in electrochemistry textbooks. However, the relationship between electrolyte and electrochemical behavior becomes less clear in high temperature, nonaqueous electrochemistry. The role of the supporting molten salt electrolyte on the electrochemical series has been observed [13], and in certain cases the changes are so severe that the series becomes inverted: a species previously thought to reduce first may now be second or third in the series [14]. These changes are not always intuitive, and optimizing separation between two electroactive species in the presence of a bulk supporting electrolyte has been the subject of many experimental studies [15–17].

To predict how the electrochemical series changes and its consequences on electrolysis, the activities of the electroactive species in both their oxidized and reduced form should be quantified. This may be accomplished through one of three main methods. The first method is direct activity measurements, such as electrochemical potential difference measurements (formerly emf). While by far the most accurate of the three methods, it requires multiple experiments at various temperatures and concentrations to accurately map out the system. In addition, all direct activity experiments require a thermodynamic and electrochemical reference. This is particularly challenging for certain high temperature molten electrolytes, such as chlorides, fluorides, and sulfides, which tend to react not only with a reference or ion-selective membrane, but also with containment, introducing further experimental unknowns.

The second method for quantifying activity is employing first-principles calculations such as density functional theory (dft). While first-principles calculations have generated a lot of excitement due to their promise in linking atomic-level phenonoma to macroscopic materials properties, they struggle to calculate entropic interactions that are important in high temperature liquids.

The final method for quantifying activity is the CALPHAD method (CALculation of PHAse Diagrams) [18]. The CALPHAD method is unique in that it

takes experimental measurements and fits them to equations of statistical thermodynamics or linear expansions of classical thermodynamics. It then generates an expression of total Gibbs energy, from which thermodynamic properties may be derived. It is fundamentally an interpolation method, and thus has difficulty predicting properties in areas far from the original interpolation, or in systems where limited data is available.

All three methods for quantifying activity have their relative strengths and weaknesses. For certain electrolytes that are high temperature, reactive, and understudied, these weaknesses overlap and frustrate attempts to understand these solutions' thermodynamic properties. An alternative method tailored to the challenges of high temperature electrolytes is needed. In his paper "The conversion of phase diagrams of solid solution type into electrochemical synthesis diagrams for binary metallic systems on inert cathodes", G. Kaptay proposed a type of phase diagram, called an "equilibrium electrochemical synthesis diagram" (eesd), which links the equilibrium relationship between metals in the cathode to the reduction potential of the electrolyte. [8]. Kaptay's work focused on the theoretical aspect of eesd derivation, which he derived for an ideal binary solution, although equations were also shown regarding application to real solutions.

Equilibrium electrochemical synthesis diagrams link easily observable results such as cathode composition to the less obvious thermodynamic properties of a novel electrolyte. The premise arises from the isothermal, isobaric thermodynamic equilibrium between two solutions. As seen in Figure 1a, two solutions α and β, both containing elements A and B, and separated by a hypothetical permeable membrane allowing A and B to pass through, may be considered to be in chemical equilibrium, where $\mu_i^\alpha = \mu_i^\beta$ and i represents A or B [19]. If one measures the chemical potential μ_A^α, they will also have measured μ_A^β, and can use the Gibbs-Duhem relation to calculate μ_B^α and μ_B^β. Figure 1b shows an extension of this case, where in order to cross the permeable membrane, elements A and B must undergo a redox reaction. The chemical potentials of A and B

in α and β are now linked by the relationship:

$$\mu_A^\beta + \mu_X^\beta - \mu_{AX}^\alpha = \Delta G_A^r \tag{4}$$

$$\Delta E_A^r = -\frac{\Delta G_A^r}{nF} \tag{5}$$

Where ΔE_A^r is the electrochemical potential of the reduction reaction $AX \rightarrow A + X$, with X being the species oxidized at the anode and A being the species reduced at the cathode (Eq. 1 - 2). μ_{AX}^α, the chemical potential of species AX in α (electrolyte), is an unknown quantity that is a function of two independent variables, μ_A^β and ΔE^r. With two unknowns and one equation (Equation 4), μ_{AX}^α cannot be determined. If the second species, B, is reducing as well, then there will be a unique potential E_S at which the co-reduction of both elements A and B takes place, as shown in Figure 2. If the mixing of A and B are energetically favored, then co-reduction of A and B will lower the Gibbs energy of reaction such that E_S takes place at a more positive potential than either E_A or E_B alone. By taking this mixing behavior into account, it is possible to link the *difference* between E_A^r and E_B^r to the $\Delta G_{A,B}^{mix}$ in β (cathode). The derivation of this relationship is given in [8], and leads to:

$$\Delta E_S = \frac{x_B * n_B * F * \Delta E_B - \Delta G_{A,B}^{mix}}{F[x_B n_B + (1 - x_B) n_A]} \tag{6}$$

where $\Delta E_B = E_B - E_A$, (i.e. the difference between B and A on the electrochemical series), $\Delta E_S = E_S - E_A$, and n_i are the number of electrons required to reduce species i.

If ΔE_S is *maximized* as a function of concentration of A and B in the cathode, and A and B are assumed to form an ideal solution as metals, ΔE_B can be determined directly as a function of the cathode composition, written here in terms of x_B:

$$\Delta E_B = \frac{RT}{n_A n_B F}[n_B \ln x_B - n_A \ln (1 - x_B)] \tag{7}$$

This relationship is undoubtedly powerful in linking the alloying chemistries of the cathode to the properties of an unknown electrolyte, here represented by

ΔE_B. However, it is limited to cathodes that form only ideal solutions and are comprised of only A and B. In order to account for a full range of possible behavior, including phase separation between A and B and the use of additional "host" metals in the cathode, the derivation should generalized. Herein, this relationship will be re-derived for the general case of a multicomponent cathode behaving as a real solution $a_B \neq x_B$. Additionally, a new thermodynamic reference state is derived that allows one to determine the activities a_{AX} and a_{BX} directly from ΔE_B.

2. Calculations

2.1. Generalization to Actual Ternary Solution

Consider a ternary system of three elements: A, B, C. Elements A and B can be reduced from the electrolyte into the cathode, while element C is a stable cathode host which does not interact with the electrolyte. The concentration of A, the more noble element, is taken as the dependent variable so concentration can be reframed in terms of B and C only. In addition, although for this derivation C is assumed to be a single element (the cathode is modeled as three components), C can also be any compound or alloy of fixed concentration, as long as it does not contain either A or B. The Gibbs energy of mixing A, B, and C to produce a liquid cathode is given by:

$$\Delta G^{mix} = G^l - (1 - x_B - x_C)G_A^\circ - x_B G_B^\circ - x_C G_C^\circ \tag{8}$$

G_i° is the standard state Gibbs energy of pure element i at the temperature and pressure of electrolysis. G^l is the Gibbs energy of a liquid cathode phase created by alloying A, B, and C. It can be represented by

$$(1-x_B-x_C)G_A^l+x_B G_B^l+x_C G_C^l+RT[(1-x_B-x_C)\ln a_A+x_B \ln a_B+x_C \ln a_C] \tag{9}$$

Where G_i^l is the Gibbs energy of element i in the pure liquid state [1].
Element A reduces at cathode potential E_A, B at E_B, and both will co-reduce at a common potential E_S (Figure 2). Following the convention of Kaptay, A is a more "noble" species than B, reducing at less negative potentials [8]. If mixing is favorable, there will be an energetic drive for A and B to reduce together at E_S. The shift from E_A (or E_B) to E_S can therefore be directly equated to the contribution of A and B to the Gibbs energy of mixing:

$$\Delta G^{mix} = -x_B n_B F(E_S - E_B) - (1 - x_B - x_C) n_A F(E_S - E_A) + x_C \Delta G_C^{mix} \quad (10)$$

where

$$\Delta G_C^{mix} = G_C^l + RT \ln a_C - G_C^\circ \quad (11)$$

and n_i is the number of electrons necessary to reduce species i, as in Equations 1 - 3. We can expand and then simplify Equation 10 with the relations $\Delta E_B = E_B - E_A$ and $\Delta E_S = E_S - E_A$, as illustrated in Figure 2. This leads to:

$$\begin{aligned} \Delta G^{mix} = &-x_B n_B F E_S + x_B n_B F E_B - (1 - x_B - x_C) n_A F(\Delta E_S) \\ &+ x_C \Delta G_C^{mix} + (x_B n_B F E_A - x_B n_B F E_A) \end{aligned} \quad (12)$$

$$\Delta G^{mix} = -x_B n_B F \Delta E_S + x_B n_B F \Delta E_B - (1 - x_B - x_C) n_A F(\Delta E_S) + x_C \Delta G_C^{mix} \quad (13)$$

$$\Delta G^{mix} = -[(1 - x_B - x_C) n_A + x_B n_B F] \Delta E_S + x_B n_B F \Delta E_B + x_C \Delta G_C^{mix} \quad (14)$$

We can rearrange to separate ΔE_S:

$$[(1 - x_B - x_C) n_A + x_B n_B F] \Delta E_S = x_B n_B F \Delta E_B + x_C \Delta G_C^{mix} - \Delta G^{mix} \quad (15)$$

We can substitute in for ΔG^{mix} using Equation 8 and expanding G^l according to Equation 9. We also expand ΔG_C^{mix} in a similar way.

[1] If pure i is liquid at the temperature of interest, $G_i^\circ = G_i^l$. If pure i is solid, but forms a liquid solution with a cathode alloy, $G_i^\circ \neq G_i^l$

$$
\begin{aligned}
[(1-x_B-x_C)n_A + x_B n_B F]\Delta E_S = {} & x_B n_B F \Delta E_B + x_C(G_C^l - G_C^\circ + RT\ln a_C) \\
& - (1-x_B-x_C)(G_A^l - G_A^\circ + RT\ln a_A) \\
& - x_B(G_B^l - G_B^\circ + RT\ln a_B) \\
& - x_C(G_C^l - G_C^\circ + RT\ln a_C)
\end{aligned} \tag{16}
$$

Simplifying Equation 16 and solving for ΔE_S we have

$$
\begin{aligned}
&\Delta E_S \\
&= \frac{x_B n_B F \Delta E_B - x_B(G_B^l - G_B^\circ) - (1-x_B-x_C)(G_A^l - G_A^\circ) - RT(x_B \ln a_B + (1-x_B-x_C)\ln a_A)}{(1-x_B-x_C)n_A F + x_B n_B F}
\end{aligned} \tag{17}
$$

Equation 17 evaluates ΔE_S as a function of concentration of A, B, and C, while taking into account the chemical interactions caused by alloying. Because C does not interact electrochemically, its direct chemical contributions drop out of the equation, and it is only the activities of A and B that determine ΔE_S. Because A and B are alloyed with C, the contribution of C is contained in the respective activity coefficients of A and B, γ_A and γ_B. This simplification will hold for any non electroactive cathode species, meaning that more complex chemistries can be incorporated.

At a certain concentration of x_B and x_C, ΔE_S will be maximized. This is equivalent to minimizing ΔG^{mix}. For a fixed cathode host composition x_C, we can find the maximum ΔE_S with respect to x_B with the equation:

$$
\frac{\partial \Delta E_S}{\partial x_B} = 0 \tag{18}
$$

Solving for ΔE_B and simplifying gives:

$$
\Delta E_B = \frac{n_A \Delta G_B^{ss} - n_B \Delta G_A^{ss} - n_B RT \ln[(1-x_B-x_C)\gamma_A] + RT\ln[x_B\gamma_B]}{F n_A n_B} \tag{19}
$$

Where ΔG_i^{ss} refers to the change in energy when moving from the standard state of species i at a given T to a liquid state. This is the generalized version of Equation 7 that can be applied to any cathode chemistry. It details how the composition of the cathode can influence to what extent codeposition can occur. When plotting x_B against ΔE_B, an equilibrium electrochemical synthesis diagram is created. For clarity of plotting, x_B is better plotted against $-\Delta E_B$.

In this notation, more positive potential differences favor the element A with a more positive potential. In order to facilitate comparison with other equilibrium diagrams (e.g. phase diagrams), the eesd's in this paper are rotated from the original design of Kaptay, placing concentration on the x-axis. An example of an electrochemical synthesis diagram plotted in this way for a general system A and B at temperature T is given in Figure 3.

Equilibrium electrochemical synthesis diagrams provide a quantitative relationship between two metals' willingness to alloy in the cathode and the difference in the electrochemical potentials required to reduce them. Two metals with favorable mixing properties, such as Pr and Nd, will have a very steep curve, indicating that very large potential differences $|\Delta E_B| >> 0$ are needed to avoid codeposition (Figure 4). On the contrary, two metals that phase separate, such as Ni and Ag, will have a horizontal curve in the region of phase separation, and a much shallower curve overall (Figure 5). This indicates that for there to be significant codeposition, $\Delta E_B \approx 0$. The tendencies of Ni and Ag to avoid mixing in the cathode result in a higher energetic barrier to codeposition. This eesd indicates it is far easier to electrochemically separate Ag from Ni in a molten salt than it would be to separate Pr from Nd.

2.2. Deriving a New Reference State

Electrochemical synthesis diagrams, as shown in Figure 3, provide a quantitative relationship between the energetics of mixing of two metals and the difference in their electrochemical potentials. To construct a simple eesd, this potential difference, ΔE_B, is left generalized. Looking in more detail, we see ΔE_B is a function of the standard state electrochemical potentials of A and B, as well as their activity in the electrolyte, here designated by the notation a_{AX}, a_{BX}, where X is the anionic species in the electrolyte. We have:

$$-\Delta E_B = E_A - E_B = E_A^\circ - \frac{RT}{n_A F} \ln a_{AX} - (E_B^\circ - \frac{RT}{n_B F} \ln a_{BX}) \tag{20}$$

Although in most cases, the standard state electrochemical potentials E_A°

and E_B° are known, the activities a_{AX} and a_{BX} are often unknown. Direct experimental measurement of activity is possible, but difficult if codeposition of A and B is favored. In this case an ion-selective membrane must be used. If the supporting electrolyte reacts with either the membrane or the reference, the activity measurements will be compromised. Unfortunately, many high-temperature supporting electrolytes are highly reactive, and a compatible membrane or reference may not be available.

In such cases, we propose a new thermodynamic reference state. When reporting activity, two reference states are commonly used. The first, Raoultian, is the simplest mathematically. It references activity to a pure state. In such cases, as the material approaches purity ($x \to 1$), activity $a \to 1$, and the activity coefficient $\gamma \to 1$. The second, Henrian, references activity to some fixed dilution. The Henrian activity coefficient f is constant if the material is sufficiently dilute. In a Henrian reference state, $f = 1$ when x is sufficiently dilute. In this region, $a = x$[20]. Herein, we propose a third reference state, the Wagner-Allanore reference state. This reference state is derived specifically for multicomponent solutions where direct activity measurements are difficult. It is a relative reference state where the activities of two species dissolved in a complex solvent are measured relative to one another (e.g. two electroactive species in a multicomponent supporting electrolyte).

The ratios of two activities in a solution remain constant regardless of which reference state is used [20]. Therefore,

$$\frac{a_B^{WA}}{a_A^{WA}} = \frac{a_B^R}{a_A^R} \tag{21}$$

Just as $a_i^R = \gamma_i x_i$, we can define:

$$a_i^{WA} = \rho_i \chi_i \tag{22}$$

Where ρ_i is the Wagner-Allanore activity coefficient of i, and χ_i is the relative composition of i. Considering the $A - B$ pseudobinary, we define:

$$\chi_A = \frac{x_A}{x_A + x_B} \tag{23}$$

We can then expand Equation 21 as:

$$\frac{\rho_B \chi_B}{\rho_A \chi_A} = \frac{\gamma_B x_B}{\gamma_A x_A} \tag{24}$$

In this new reference state, we set $\rho_A = 1$ such that $a_A^{WA} = \chi_A$, giving:

$$\frac{\rho_B \chi_B}{\chi_A} = \frac{\gamma_B x_B}{\gamma_A x_A} \tag{25}$$

Noting that:

$$\frac{\chi_B}{\chi_A} = \frac{x_B}{x_A} \tag{26}$$

We can simplify and arrive at the relation:

$$\rho_B = \frac{\gamma_B}{\gamma_A} \tag{27}$$

Equation 27 demonstrates the utility of the this new reference state. It captures how the chemical potential of species A and B vary with respect to each other, as well as how other components in the solution may effect this relationship. For example, if A and B are dissolved into solvent C, and solvent C tends to bond with A ($\gamma_A < 1$), while phase separating with B ($\gamma_B > 1$), then $\gamma_B > \gamma_A$ and $\rho_B > 1$. In certain cases, exact calculation of γ_A and γ_B is impractical or difficult, but ρ_B can be easily measured by using an eesd diagram in combination with Equation 20. Since ρ_B is all that is needed to determine if the electrolyte solution properties favor codeposition or purification, reframing activity in this reference state is particularly useful to electrochemists. The Wagner-Allanore reference state can be converted to a Raoultian reference state via the equation:

$$a_B^R = a_B^{WA} \gamma_A \tag{28}$$

The conversion factor, γ_A is a function of composition x_A. Because the composition coordinate χ is relative as well, there are no limits on how dilute or concentrated A and B can be in the solvent. Thus, this new reference state has

several significant advantages over Raoultian and Henrian states. First, because it is a *relative* reference state, not an absolute reference, it is easier to measure experimentally, particularly when very reactive solutions are involved. Second, because it measures the pseudobinary between A and B, there are no conditions on concentration. A Raoultian reference state is the simplest mathematically and experimentally when a material is very concentrated. A Henrian reference state is the simplest mathematically and experimentally when a material is very dilute. By defining a new composition coordinate χ, species A and B can be at any dilution without losing information. Although the exact, independent activities of A or B cannot be determined, much of the information about the solution is still retained, such as how A and B interact with each other and with their solvent. Figure 6 shows a comparison between activities reported in a Raoultian, Henrian, and Wagner-Allanore reference state.

3. Model Application Results

Although production of a pure metal through electrolysis is typically achieved by using a pure feedstock or selective solvent, there are certain cases where two species are soluble and present in amounts that make codeposition possible, notably in nuclear waste processing and in rare earth metal production [1, 7, 12, 21]. In order to test the utility of equilibrium electrochemical synthesis diagrams and the Wagner-Allanore reference state, experimental results for these case studies are compared to predictions from our new model.

3.0.1. Nickel-Cobalt

The first case study focuses on nickel-cobalt separation in a LiCl-KCl molten salt electrolyte. This is an important system in the nuclear industry, where Ni steam generators are contaminated by Co-60, hindering their recyclability. Choi et. al investigated the ability to electrochemically separate Ni from Co in a molten salt solution at 823K [21]. The standard-state decomposition potential

of *liquid* $NiCl_2$ to Ni is -798mV, while the standard-state decomposition potential of *liquid* $CoCl_2$ is -998mV. Note that both $NiCl_2$ and $CoCl_2$ are solid in their pure state, yet soluble in liquid LiCl-KCl. For this reason, thermodynamics of the liquid should be used. The difference in decomposition potential between Ni and Co, $E^{\circ}_{\mathrm{Ni}} - E^{\circ}_{\mathrm{Co}}$, is 200mV. On the electrochemical synthesis diagram shown in Figure 7 a, a 200mV potential difference corresponds to approximately 0.25 $mol\%$Co alloyed into the Ni cathode.

In their investigation of reduction potential peaks through cyclic voltammetry, Choi et al measured a potential difference of 185mV when both $NiCl_2$ and $CoCl_2$ are present each at $2wt\%$ in the supporting electrolyte [21]. On an electrochemical synthesis diagram, a 185mV difference corresponds to approximately 0.37 $mol\%$Co. Chronopotentiometry experiments of this electrolyte during which electrolysis was run at 50mA, 200mA, and 500mA revealed an experimental cathode concentration of 0.22, 0.53, and 1.17 $mol\%$Co. Figure 7 b compares the Wagner-Allanore activity coefficient calculated for each experiment, compared with the predicted coefficient from the synthesis diagram. There is strong agreement between the predicted activity coefficient and that measured with a low current density (50mA). As current density increases, the amount of Co in the Ni cathode increases, and the measured activity coefficient strays from its equilibrium thermodynamic prediction.

3.0.2. Praseodymium-Neodymium

The second case study, praseodymium-neodymium alloy production from a mixed rare earth oxide, was chosen for several notable reasons. First, Pr-Nd electrolysis takes place in a molten fluoride electrolyte into which Nd_2O_3 and Pr_2O_3 are dissolved. The anion here is the oxide ion, which is different from the anion of the supporting electrolyte, the fluoride ion. The additional interactions between the two anions create additional complications that hinder modeling efforts and frustrate attempts to measure thermodynamic properties. By reframing the solution properties of the oxyfluoride electrolyte into the relative Wagner-Allanore reference state, this confusion is easily avoided and the ener-

getic effect the molten fluoride has on the dissolved oxide species is captured by ρ. Second, the conditions under which Pr-Nd electrolysis take place are proprietary, with few papers available discussing the process in sufficient detail [12]. Without information about the actual electrolyte composition used, and with process conditions (temperature, current density, atmosphere) unknown, it is difficult to replicate the conditions in a laboratory setting in order to gather thermodynamic data. Commercially available CALPHAD models of the electrolyte are limited to binary fluoride systems, and even then, available models are extrapolated from the data of better understood systems [22]. An alternate method of investigating the thermodynamic properties of this electrolyte would clearly aid researchers in understanding more about Pr-Nd alloy production methods.

The Pr-Nd metallic system is well enough understood to build a binary CALPHAD model (Figure 4), which can be used to generate an electrochemical synthesis diagram for the system. At 1323K, standard state decomposition potential of *liquid* Pr_2O_3 to *liquid* Pr is -2.363V, while the standard state decomposition potential of *liquid* Nd_2O_3 to *liquid* Nd is -2.372V. The difference in potentials between Pr and Nd, $\Delta E_{\mathrm{Pr}} - \Delta E_{\mathrm{Nd}}$, is 8mV. On an electrochemical synthesis diagram, a 8mV potential difference corresponds to approximately 45 *mol*%Nd alloyed into the Pr cathode (Figure 8). For an oxide composition ratio 66 *mol*%Nd - 33 *mol*%Pr, a cathode composition of 71 *mol*%Nd - 29 *mol*%Pr was measured [1]. Despite Pr occupying a more cathodic potential on the standard state electropotential series, the cathode was more enriched in Nd. From this data, $\rho_{\mathrm{Nd_2O_3}}$ is calculated to be 4.8. $\rho_{\mathrm{Nd_2O_3}} > 1$ shows an energetic penalty to mix Nd_2O_3 in the electrolyte relative to Pr_2O_3.

4. Discussion

4.1. Nickel-Cobalt

Figure 7 compares the amount of Co predicted in the Ni cathode after electrolysis with experimental results. The predicted value of 0.25 $mol\%$ is calculated using an eesd that relates $E_{\mathrm{Ni}} - E_{\mathrm{Co}}$ to the thermodynamics of a Ni-Co alloy. Without experimental data, $E_{\mathrm{Ni}} - E_{\mathrm{Co}}$ is unknown, however, it can be approximated by using the standard state values $E^{\circ}_{\mathrm{Ni,l}}$ and $E^{\circ}_{\mathrm{Co,l}}$. A liquid standard state takes into account the change in Gibbs energy upon dissolving solid $NiCl_2$ and $CoCl_2$ into molten chloride electrolyte. Even when there is no information available regarding the electrolyte, using an eesd allows one to take into account the contribution of Ni-Co mixing in the cathode. The value this additional information can be seen in the agreement between the predicted value of 0.25 $mol\%$ Co and the experimental value of 0.22 $mol\%$Co achieved during low current density electrolysis.

The difference between the measured reduction potentials of Co and Ni during cyclic voltammetry is 225mV, corresponding to 0.37 $mol\%$Co in Ni. This is slightly higher than provided by the standard state case, and higher than the composition measured after electrolysis at 50mA. Without data on the equilibrium exchange between Co and Ni in molten chloride, one cannot determine if this difference is due to solution interactions or kinetic and mass transport effects that arose during electrochemical operation. However, there is some evidence to suggest that non-thermodynamic effects play a non-negligible role in the final experimental result. First, Ni-Co alloy is solid at 823K, which will inevitably hinder diffusion of Co into Ni and effect the alloy chemistry. This is one possible reason why the 50mA case is lower than both model predictions. Furthermore, higher current density during electrolysis corresponds to higher concentration of Co in the cathode (Fig. 7). Higher current densities during electrolysis can push the cell into an operation regime limited by mass-transfer. If there is locally increased concentration of $CoCl_2$ in the vicinity of the cathode, for example, then ρ_{CoCl_2} will be higher at the electrode interface than in

the bulk solution. In fact, as current density increased from 50mA to 500mA, calculated ρ_{CoCl_2} was observed to increase correspondingly.

4.2. Praseodymium-Neodymium

Although considerably less information is available on Pr-Nd alloy production through electrolysis, important insights can be gained by comparing model predictions to published data. Figure 8 shows more Nd was reduced than Pr, although Pr is the more cathodic metal. There are several reasons this may occur. First, from the experimental data, $\rho_{Nd_2O_3} \approx 4.8$. If this value is representative of equilibrium conditions, then there is an energetic penalty for mixing Nd_2O_3 into the electrolyte. Since the value of this increased Gibbs energy of mixing is measured relative to Pr_2O_3, there is a driving force to reduce the concentration of Nd_2O_3 in the electrolyte while increasing the concentration of Pr_2O_3. This will result in increased production of Nd metal.

An alternative explanation considers that although Pr is the more cathodic metal on the electropotential series for *oxides*, Nd is the more cathodic metal for the fluoride series. Both PrF_3 and NdF_3 are present in the fluoride supporting electrolyte [12]. If PrF_3 and NdF_3 were being reduced preferentially instead of the oxides, a more Nd-rich alloy would be the result. However, in order for rare earth fluorides to be reduced in steady state, the fluoride ion should be oxidized at the anode, typically producing perfluorinated compounds (PFC) when the electrolyte is a molten oxyfluoride. Literature studying PFC emissions in Pr-Nd electrolysis cells have noted that they are on average 2-3 orders of magnitude lower than CO_2 production [12, 23]. Even if all PFC emissions were the result of NdF_3 electrolysis, there would not be enough Nd produced from fluoride to account for the change in cathode composition.

A final explanation for the increased production of Nd could be the result of mass transport limitations inside the electrolysis cell. Nd_2O_3 is present at nearly double the concentration of Pr_2O_3. At the high current densities used for electrolysis, it is entirely plausible that in the vicinity of the cathode, there was an even greater concentration difference between Nd_2O_3 and Pr_3O_3 [12]. This ex-

planation concurs with the results of the Ni-Co case, where concentration of Co was noted to increase with current density. Furthermore, available thermodynamic models for the $LiF - PrF_3$ system and the $LiF - NdF_3$ system suggest Nd and Pr behave similarly in the electrolyte, which would result in an equilibrium $\rho \approx 1$. It is critical to note, however, that this is only for the thermodynamics of the molten fluorides. To the author's knowledge, there is currently no commercially available data, experimental or modeled, for the $Pr - Nd - O$ system. Further experimental investigation is necessary in order to determine if Nd enrichment in the electrolyte is the result of thermodynamic or transport phenomena.

5. Conclusion

As the drive for more innovative electrochemical technologies increase, so will the use of new and understudied electrolytes. When insufficient experimental data is available, it is common to approximate that electrolytes will exhibit standard state or ideal solution behavior. Without any quantitative model for when codeposition will occur in electrolysis, issues of cathode contamination are often avoided entirely by pre-purifying electrochemical feedstock or limiting the electrolyte to solutions previously studied and understood to be selective by nature. By considering the thermodynamic properties of the electrolyte and cathode solutions, and understanding how these properties will govern interactions between the two solutions, new insights on which alloy will be produced during electrolysis may be gained. By generalizing the theory of electrochemical synthesis diagrams to accommodate any solution, the relationship between reduction potential and cathode metallurgy can be elucidated. By re-framing the activity of electrolytes into a new, relative reference state, synthesis diagrams can be used as a tool to directly probe the thermodynamic properties of electrolytes, a task that was previously frustrated by the complex and reactive nature of these electrolytes. As seen in two different case studies, use of synthesis diagrams in conjunction with the Wagner-Allanore reference state allows the

experimentalist the opportunity to gain new insights into the behavior of their system, and to use those insights to guide further development.

6. Acknowledgements

The authors gratefully acknowledge the National Science Foundation (CMMI Project 1760025) for their support of this research endeavor.

7. References

[1] K. Milicevic, T. Meyer, B. Freidrich, Influence of electrolyte composition on molten salt electrolysis of didymium, in: ERES2017: 2nd European Rare Earth Resources Conference, Santorini, 2017. doi:10.13140/RG.2.2.13137.33122.

[2] J. Metson, Production of Alumina, in: R. Lumley (Ed.), Fundamentals of Aluminum Metallurgy, Woodhead, Cambridge, 2011, Ch. 2, pp. 23–48.

[3] W. Davenport, M. King, M. Schlesinger, A. Biswas, Extractive Metallurgy of Copper, 4th Edition, Elsevier Science, 2002.

[4] S. Sokhanvaran, S.-K. Lee, G. Lambotte, A. Allanore, Electrochemistry of Molten Sulfides: Copper Extraction from BaS-Cu 2 S, Journal of The Electrochemical Society 163 (3) (2016) D115–D120. doi:10.1149/2.0821603jes.

[5] S. K. Sahu, B. Chmielowiec, A. Allanore, Electrolytic Extraction of Copper, Molybdenum and Rhenium from Molten Sulfide Electrolyte, Electrochimica Acta 243 (2017) 382–389. doi:10.1016/j.electacta.2017.04.071.

[6] A. Allanore, Features and Challenges of Molten Oxide Electrolytes for Metal Extraction Fundamentals of Metal Extraction: The Electrolytic Path, Journal of The Electrochemical Society 162 (1) (2015) 13–22. doi:10.1149/2.0451501jes.

[7] J. P. Ackerman, W. E. Miller, Electrorefining process and apparatus for recovery of uranium and a mixture of uranium and plutonium from spent fuels (nov 1989).

[8] G. Kaptay, The conversion of phase diagrams of solid solution type into electrochemical synthesis diagrams for binary metallic systems on inert cathodes, Electrochimica Acta 60 (2012) 401–409. doi:10.1016/j.electacta.2011.11.077.

[9] A. N. Baraboshkin, Elektrocrystalization from Molten Salts, Nauka, Moscow, 1976.

[10] V. V. Malyshev, H. B. Kushkhov, V. I. Shapoval, High-temperature electrochemical synthesis of carbides, silicides and borides of VI-group metals in ionic melts, Journal of Applied Electrochemistry 32 (2002) 573–579.

[11] H. Kvande, Production of Primary Aluminum, in: R. Lumley (Ed.), Fundamentals of Aluminum Metallurgy, 1st Edition, Woodhead Publishing, 2010, Ch. 3, pp. 49–69.

[12] K. Milicevic, D. Feldhaus, B. Friedrich, Conditions and mechanisms of gas emissions from didymium electrolysis and its process control, in: Minerals, Metals and Materials Series, Vol. Part F4, Springer International Publishing, 2018, pp. 1435–1441. doi:10.1007/978-3-319-72284-9_187.

[13] A. Cox, D. Fray, Separation of Mg and Mn from Beverage Can Scrap using a Recessed-Channel Cell, Journal of The Electrochemical Society 150 (12) (2003) D200–8. doi:10.1149/1.1623768.

[14] T. Lichtenstein, T. P. Nigl, N. D. Smith, H. Kim, Electrochemical deposition of alkaline-earth elements (Sr and Ba) from LiCl-KCl-SrCl 2 -BaCl 2 solution using a liquid bismuth electrode, Electrochimica Acta 281 (2018) 810–815. doi:10.1016/j.electacta.2018.05.097.

[15] J. P. Ackerman, J. L. Settle, Partition of lanthanum and neodymium metals and chloride salts between molten cadmium and molten LiCl-

KCl eutectic, Journal of Alloys and Compounds 177 (1991) 129–141. doi:10.1016/0925-8388(91)90063-2.

[16] J. P. Ackerman, J. L. Settle, Distribution of plutonium, americium, and several rare earth fission product elements between liquid cadmium and LiCl-KCl eutectic, Journal of Alloys and Compounds 199 (1993) 77–84. doi:10.1016/0925-8388(93)90430-U.

[17] Y. Sakamura, O. Shirai, T. Iwai, Y. Suzuki, Distribution behavior of plutonium and americium in LiCl–KCl eutectic/liquid cadmium systems, Journal of Alloys and Compounds 321 (2001) 76–83. doi:10.1016/S0925-8388(01)00973-2.

[18] C. W. Bale, E. Bélisle, P. Chartrand, S. A. Decterov, G. Eriksson, A. E. Gheribi, K. Hack, I. H. Jung, Y. B. Kang, J. Melançon, A. D. Pelton, S. Petersen, C. Robelin, J. Sangster, P. Spencer, M. A. Van Ende, FactSage thermochemical software and databases, 2010-2016, Calphad 54 (2016) 35–53. doi:10.1016/j.calphad.2016.05.002.

[19] L. Palatnik, A. Landau, Phase Equilibria in Multicomponent Systems, Holt, Rinehart, and Winston, Inc., New York, 1964.

[20] C. H. P. Lupis, Chemical Thermodynamics of Materials, North-Holland, New York, 1983.

[21] W. S. Choi, S. H. Cho, Y. J. Lee, Y. S. Kim, J. H. Lee, Separation behavior of nickel and cobalt in a LiCl-KCl-NiCl2 molten salt by electrorefining process, Journal of Electroanalytical Chemistry 866. doi:10.1016/j.jelechem.2020.114175.

[22] J. P. Van Der Meer, R. J. Konings, M. H. Jacobs, H. A. Oonk, Thermodynamic modelling of LiF-LnF3 and LiF-AnF3 phase diagrams, Journal of Nuclear Materials 335 (3) (2004) 345–352. doi:10.1016/j.jnucmat.2004.07.035.

[23] L. Zhang, X. Wang, B. Gong, Perfluorocarbon emissions from electrolytic reduction of rare earth metals in fluoride/oxide system, Atmospheric Pollution Research 9 (1) (2018) 61–65. doi:10.1016/j.apr.2017.06.006.

8. Figures

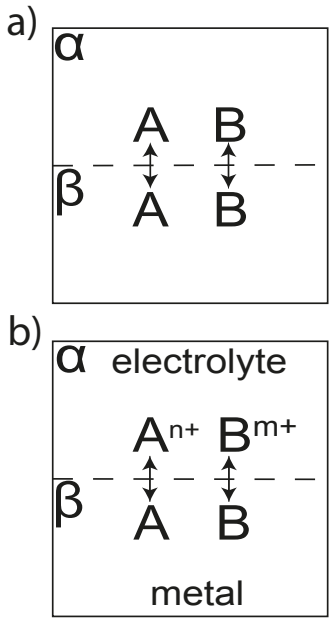

Figure 1

Figure 1 a) exchange of species A and B through a permeable membrane separating solutions α and β. b) species A and B must undergo a redox reaction in order to exchange between the metal and electrolyte

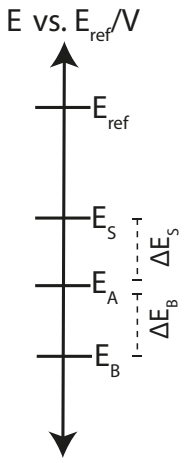

Figure 2

Figure 2 Hypothetical placement of E_A, E_B, and E_S on electrochemical potential series. In this example, $E_{ref} = 0$.

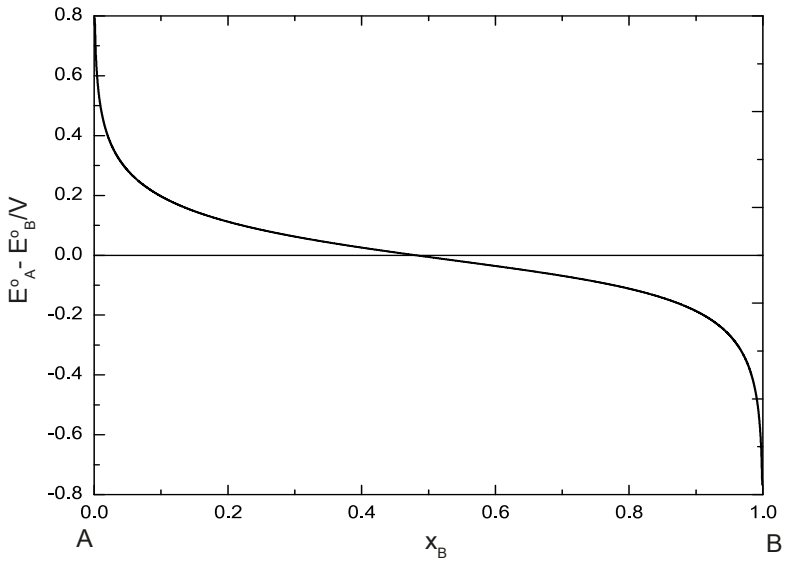

Figure 3

Figure 3 Equilibrium electrochemical synthesis diagram for an arbitrary binary system A-B, where A is the more noble element on the electrochemical potential series, and A and B form a completely miscible metallic solution.

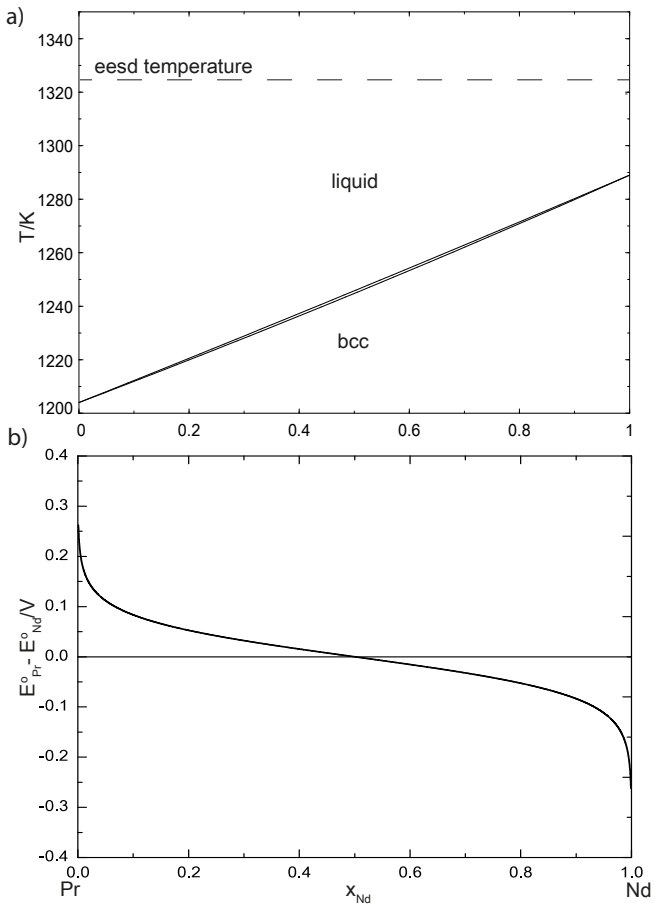

Figure 4

Figure 4 Equilibrium electrochemical synthesis diagram for the Pr−Nd/Pr_2O_3−Nd_2O_3 system at 1323K. At this temperature, Pr and Nd form a completely miscible liquid.

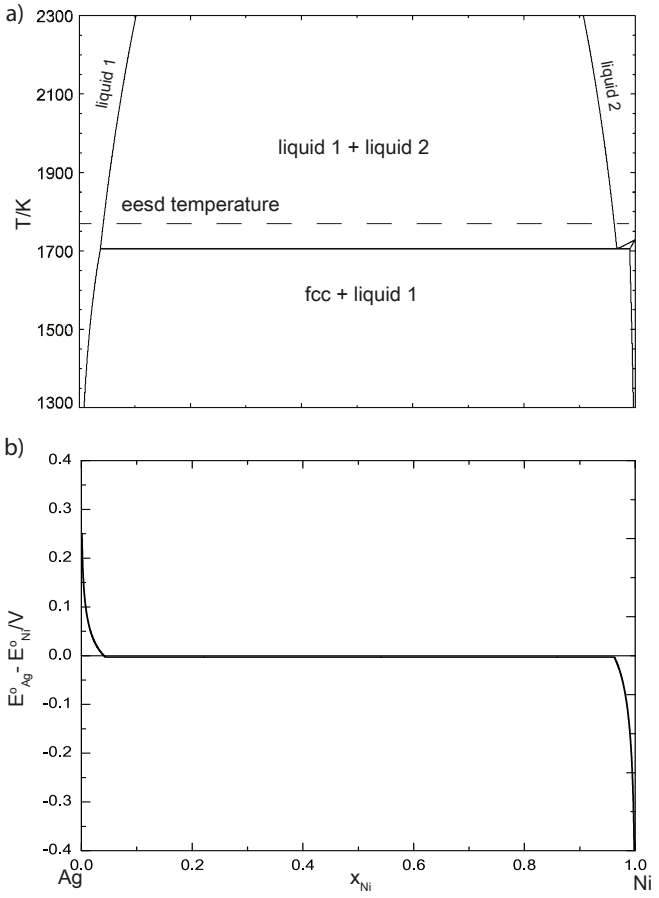

Figure 5

Figure 5 Equilibrium electrochemical synthesis diagram for the Ag−Ni/$AgCl_2$−$NiCl_2$ system at 1773K. At this temperature, Ag and Ni phase separate to form two different liquid solutions.

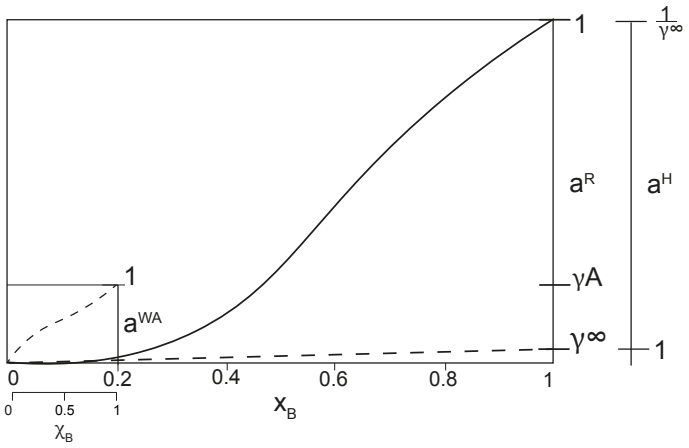

Figure 6

.

Figure 6 Comparison of Raoultian, Henrian, and Wagner-Allanore reference states. Henrian activities are scaled according to the value of γ_∞, while Wagner-Allanore activities are scaled according to the activity coefficient of A, γ_A, which may not be constant with concentration, unlike in the Henrian case. The composition coordinate of the Wagner-Allanore reference state is also rescaled along the $A - B$ pseudobinary

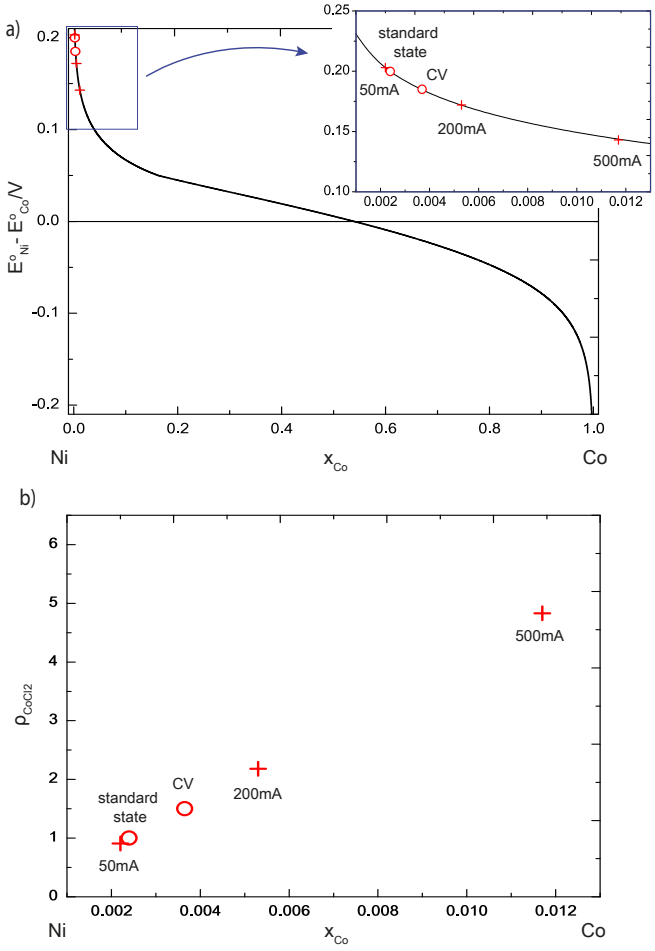

Figure 7

Figure 7 a) Electrochemical synthesis diagram for $Ni - Co/NiCl_2 - CoCl_2$ system at 823K. b) Wagner-Allanore activity coefficient ρ for $CoCl_2$. O: Values calculated for: $E^{\circ}_{\mathrm{Ni}} - E^{\circ}_{\mathrm{Co}} = 0.2V$ (from standard state), and $E^{\circ}_{\mathrm{Ni}} - E^{\circ}_{\mathrm{Co}} = 0.185V$ (from cyclic voltammetry peaks). +: experimental concentration of Co in Ni cathode after chronopoteniometry at $50mA/cm^2$, $200mA/cm^2$, and $500mA/cm^2$ [21]

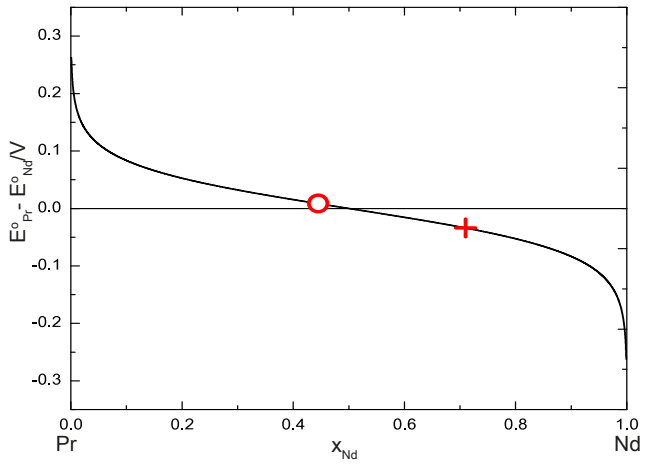

Figure 8

Figure 8 Electrochemical synthesis diagram for for the $\mathrm{Pr} - \mathrm{Nd}/\mathrm{Pr_2O_3} - \mathrm{Nd_2O_3}$ system at 1323K with: O: predicted concentration of Nd in Pr based on $E^{\circ}_{\mathrm{Pr}} - E^{\circ}_{\mathrm{Nd}} = 0.008V$, +: calculated from experimental results [1]

9. List of Captions

Figure 1 a) exchange of species A and B through a permeable membrane separating solutions α and β. b) species A and B must undergo a redox reaction in order to exchange between the metal and electrolyte

Figure 2 Hypothetical placement of E_A, E_B, and E_S on electrochemical potential series. In this example, $E_{ref} = 0$.

Figure 3 Equilibrium electrochemical synthesis diagram for an arbitrary binary system A-B, where A is the more noble element on the electrochemical potential series, and A and B form a completely miscible metallic solution.

Figure 4 Equilibrium electrochemical synthesis diagram for the $\mathrm{Pr}-\mathrm{Nd}/\mathrm{Pr_2O_3}-\mathrm{Nd_2O_3}$ system at 1323K. At this temperature, Pr and Nd form a completely miscible liquid.

Figure 5 Equilibrium electrochemical synthesis diagram for the $\mathrm{Ag}-\mathrm{Ni}/\mathrm{AgCl_2}-\mathrm{NiCl_2}$ system at 1773K. At this temperature, Ag and Ni phase separate to form two different liquid solutions.

Figure 6 Comparison of Raoultian, Henrian, and Wagner-Allanore reference states. Henrian activities are scaled according to the value of γ_∞, while Wagner-Allanore activities are scaled according to the activity coefficient of A, γ_A, which may not be constant with concentration, unlike in the Henrian case. The composition coordinate of the Wagner-Allanore reference state is also rescaled along the $A - B$ pseudobinary

Figure 7 a) Electrochemical synthesis diagram for $\mathrm{Ni} - \mathrm{Co}/\mathrm{NiCl_2} - \mathrm{CoCl_2}$ system at 823K. b) Wagner-Allanore activity coefficient ρ for $\mathrm{CoCl_2}$. O: Values calculated for: $E^\circ_{\mathrm{Ni}} - E^\circ_{\mathrm{Co}} = 0.2V$ (from standard state), and $E^\circ_{\mathrm{Ni}} - E^\circ_{\mathrm{Co}} =$

$0.185V$ (from cyclic voltammetry peaks). ✛: experimental concentration of Co in Ni cathode after chronopoteniometry at $50mA/cm^2$, $200mA/cm^2$, and $500mA/cm^2$ [21]

Figure 8 Electrochemical synthesis diagram for for the $Pr - Nd/Pr_2O_3 - Nd_2O_3$ system at 1323K with: O: predicted concentration of Nd in Pr based on $E^{\circ}_{Pr} - E^{\circ}_{Nd} = 0.008V$, ✛: calculated from experimental results [1]